PCCP

Improving the Theoretical Description of Ln(III)/An(III) Separation with Phosphinic Acid Ligands: A Benchmarking Study of Structure and Selectivity

Journal:	*Physical Chemistry Chemical Physics*
Manuscript ID	CP-ART-06-2021-002466.R1
Article Type:	Paper
Date Submitted by the Author:	03-Aug-2021
Complete List of Authors:	Chapleski, Robert; University of Tennessee Knoxville, Chemistry Ivanov, Alexander; Oak Ridge National Laboratory, Chemical Sciences Division Peterson, Kirk; Washington State University, Department of Chemistry; Bryantsev, Vyacheslav; Oak Ridge National Laboratory, Chemical Sciences Division

ARTICLE

Improving the Theoretical Description of Ln(III)/An(III) Separation with Phosphinic Acid Ligands: A Benchmarking Study of Structure and Selectivity

Received 00th January 20xx,
Accepted 00th January 20xx

DOI: 10.1039/x0xx00000x

Robert C. Chapleski, Jr.,[a] Alexander S. Ivanov,[a] Kirk A. Peterson,*[,b] Vyacheslav S. Bryantsev*[,a]

The efficient separation of trivalent lanthanides from minor actinides with soft-donor ligands, while showing experimental promise, has theorists continuing to search for suitable approaches for describing and interpreting selectivity. To remedy this, we employ several computational methods in describing the structure of model $M(H_2PX_2)_3$ complexes, with M=Eu and Am, and X=O, S, Se, and Te, and predicting the selectivity of model phosphinic acid ligands in Eu(III)/Am(III) separation. After first establishing a set of MP2 and CCSD(T)-DKH3 results as benchmarks, we evaluate several density functionals and descriptions of valence shells for their accuracy with respect to metal—ligand bonding and selectivity. We find that commonly employed functionals with a 0-27% range of exact exchange used with small-core effective core potentials or with an explicit treatment of the relativistic effects (DKH2) incorrectly predict a decrease in the metal-ligand bond distance in going from Eu(III) to Am(III) and completely fail to track a selectivity trend, even giving a wrong sign for some or all ligands. Surprisingly, when these functionals are used in conjunction with an f-in-core description of metal ions, the correct trend in selectivity is recovered, though Am—X distances are overestimated in relation to Eu—X. Functionals with high components of exact exchange (50%) and double-hybrid functionals are reasonably aligned with benchmark results, pointing to the problems of DFT with small exact exchange fractions to handle f-electrons. Natural bond orbital analyses reveal that these poorly performing functionals disproportionately overpopulate outer f orbitals in the model complexes. We anticipate that recommendations resulting from this work will lead to more accurate theoretical descriptions of lanthanide/actinide selectivity with soft-donor chalcogen-based ligands in the future.

Introduction

With the advent of applied nuclear technology in the early 20th century came the eventual need to safely handle and dispose of consequent radionuclides, incorporated within spent fuel products over extended periods of time. Early efforts recognized that the separation of especially radioactive species from less harmful ones could facilitate the efficient disposal and potential recycling of these products for future use. For example, slow-decaying minor-actinide ions, including Am(III) and Cm(III)—products of the transmutation of uranium and plutonium in applied energy release—show promise for use in molten salt reactors for further power generation.[1] The realization of potential applications necessitates the separation of these minor actinides from lanthanide species, as the large neutron-capture cross-sections of the latter would reduce transmutation efficiency of the former. Additionally, the sequestration of highly radioactive minor actinides from spent fuels would mitigate the long-term hazards and thermal heat load associated with long-lived fission products. However, due to similar ionic radii of actinides and lanthanides, this process is far from facile. After initial efforts, however, in 1996, Jiao and co-workers[2, 3] found that the dithiophosphinic acid compound Cyanex-301, a main component of which is bis(2,4,4-trimethylpentyl)dithiophosphinic acid, effectively led to the separation of Am(III) ions from lanthanide Eu(III) in a liquid-liquid separation process, with a separation factor of almost 6000. In light of promising experimental results, theoretical approaches have undertaken the task of understanding the molecular-scale phenomena leading to lanthanide/actinide separation by soft-donor phosphinic acid ligands such as Cyanex-301. Two main areas of focus have been the structures of metal-ligand complexes and reaction energies describing selectivity.

Structural descriptions of soft donor ligand—f-metal complexes of lanthanides and minor actinides resulting from computational approaches have shown varying degrees of success. Experimental extended x-ray adsorption fine structure (EXAFS) spectra reveal longer metal—sulfur bond distances in Cyanex-301 complexes of Am(III) (2.98 Å)[4] than Eu(III) (2.84 Å)[5], although different coordination structures and extraction environments are noted for both complexes (i.e., 4:1 Am—Cyanex-301 via coordination of eight sulfur atoms, in hydrogenated kerosene, and 4:1 Eu—Cyanex-301 via coordination of seven sulfur atoms and an oxygen from a water molecule, in toluene). Further, EXAFS structures of 3:1 Cyanex-301

[a] Chemical Sciences Division, Oak Ridge National Laboratory, 1 Bethel Valley Road, Oak Ridge, TN 27831, USA, E-mail: bryantsevv@ornl.gov
[b] Department of Chemistry, Washington State University, Pullman, WA 99164, USA, E-mail: kipeters@wsu.edu

Electronic Supplementary Information (ESI) available: Additional MP2 reaction energies, second-order stabilization energies, additional basis functions for core-valence basis sets, recontracted basis sets for Eu(III) and Am(III) and spatial coordinates for all structures. See DOI: 10.1039/x0xx00000x

complexes show longer metal—sulfur distances for trivalent Cm complexes (d(Cm—S) = 2.826 Å) than for Sm (d(Sm—S = 2.803 Å)).[6, 7] This difference in bond distances aligns with the larger radius of the Cm(III) ion (i.e., r_{Cm} = 1.11 Å) than the Sm(III) ion (r_{Sm} = 1.098 Å). An x-ray diffraction study of aromatic thiophosphinic Eu(III) and Am(III) complexes shows almost identical metal—S bond lengths within experimental error (i.e., 2.910 ± 0.009 Å for the Eu(III) complex, and 2.921 ± 0.009 Å for the Am(III)), although the ionic radius of Am(III) (r_{Am} = 0.975 Å) is larger than that of Eu(III) (r_{Eu} = 0.947 Å). [8, 9] While close distances have been reported, we find no instance of a distinguishably shorter metal—soft-donor distance in an Am(III) complex than in an analogous Eu(III) complex. Initial efforts to describe the structures of dithiophosphinic—trivalent-f-metal complexes from a theoretical perspective by the Kaltsoyannis group[10-12] enlisted the PBE density functional along with a small-core effective-core-potential (SC ECP) description of metal ions, in which outer f-electrons are included explicitly within the valence shell. For 3:1 complexes of $N(XPR_2)_2$ ligands, where X = O, S, Se, and Te, with various lanthanides and actinides, their results generally showed significantly smaller average metal—X bond lengths in actinide complexes than in lanthanide complexes with soft donor ligands (i.e., X = S, Se, and Te), in contrast with experimental results for Cyanex-301 complexes. Specifically, for R = H complexes, d(Eu—S) = 2.873 Å and d(Am—S) = 2.835 Å; d(Eu—Se) = 2.985 Å and d(Am—Se) = 2.940 Å; and d(Eu—Te) = 3.20 Å and d(Am—Te) = 3.149 Å. In 2011, Bhattacharyya et al.[13] calculated structures for 3:1 ligand—metal complexes formed with the model $Me_2PS_2^-$ ligand, using a variety of pure density functionals: BP86, PW91, BLYP, and PBE, and an SC ECP description of f-metal ions. Results for all functionals tested revealed similar, yet shorter, Am—S distances (ranging from 2.827 (PW91) to 2.890 Å (BLYP)) in comparison to Eu—S distances (2.839 (PW91) to 2.899 Å (BLYP)).

Highlighting discrepancies amongst Am/Eu—soft-donor-ligand interatomic distances obtained from previous theoretical studies, and particularly considering the finding of shorter Am—S than Eu—S bond lengths from SC ECP DFT studies, which contrast experimental EXAFS and XRD structures,[4-7, 9, 10] Dolg et al.[14] compared SC ECP structures of 3:1 model-dithiophosphinic-acid Eu/Am complexes resulting from calculations with the BP86 functional with those from unrestricted Hartree-Fock (UHF) and MP2 calculations. For all complexes, shorter, yet similar, Am—S distances (2.830 to 2.846 Å) were found in comparison to Eu—S distances (2.857 to 2.879 Å) from density functional calculations, while longer, yet similar, distances were obtained from UHF (Am—S: 2.916 to 2.927 Å; Eu—S: 2.873 to 2.881 Å) and MP2 methods (Am—S: 2.750 to 2.767 Å; Eu—S: 2.728 to 2.744 Å). The authors of this 2014 work suggest that the discrepancy in metal—soft-atom distance trends results from the delocalization (i.e., self-interaction) error inherent to several density functionals, when f electrons are treated explicitly. To alleviate the problem of self-interaction error, they recommended an approach that includes a high admixture of Hartree-Fock exchange (E_X^{HF}) into a DFT description, recovering the correct trend in Am—S and Eu—S distances. A similar improvement in the prediction of the Am—S and Eu—S bond distances in the 3:1 Cyanex-301 complexes by the same authors was achieved[15] using a large-core effective-core-potential (LC ECP) description, wherein metal f-electrons were included within the relativistic pseudopotential. The problem of an unphysical overfilling of the 4f shell of Eu(III) was first observed by Dolg[16] in a study of EuX_3 (X=F,Cl,Br,I) using all-electron DKH2 PBE0 calculations, pointing to a general problem of open f shell description in lanthanides with conventional DFT methods.

Despite findings by Dolg et al.,[14,16] many groups continued to enlist pure density functional approaches for describing soft-donor—trivalent-f complexes. Recent work used SC ECP approaches with the PBE and BP86 functionals to describe the $Am(Me_2PS_2)_3$[17] and $Eu(Cyanex\text{-}301)_3$[18,19] complexes, respectively. Kaneko et al.[20,21] performed a series of studies on Eu/Am—Me_2PS_2 complexes using the BP86 functional, now with an all-electron approach to describing the lanthanide and actinide ions. Even with the explicit description of all orbitals with all-electron relativistically contracted basis sets, shorter, yet similar, average Am—S distances were found (2.839 Å) in comparison to Eu—S (2.844 Å).[20,21] In a follow-up study to earlier computational work by the Kaltsoyannis group,[10-12] Kaneko and Watanabe[22] also investigated 3:1 complexes of $N(XPMe_2)_2^-$ ligands, now enlisting their BP86/SARC/ZORA approach. In line with Kaltsoyannis' PBE/SC ECP results, [10-12] Kaneko and Watanabe[22] found shorter, yet similar, Am—X distances to Eu—X for soft-donor X atoms (i.e., Am—S: 2.831 Å, Eu—S 2.849 Å; Am—Se: 2.952 Å, Eu—Se: 2.971 Å; Am—Te: 3.144 Å, Eu—Te: 3.176 Å). More recently, Pu and co-workers[23] used the B3LYP hybrid functional, which includes a 20% E_X^{HF}, with SC ECP to determine structures of 3:1 complexes of aryl dithiophosphinic acids with increasing degrees of trifluoromethyl substitution, still finding shorter Am—S distances for ligand complexes with low substitution. Only when Wang et al.[24] used the M06-2X density functional, thereby increasing E_X^{HF} to 56%,[25] along with a SC ECP, were longer Am—S distances than Eu—S distances in complexes with Me_2PS_2 ligands found. This result marks a clear contrast with the SC ECP studies using functionals without exact exchange, i.e., PBE, BP86, PW91, and BLYP, and functionals with a small E_X^{HF} fraction such as B3LYP, all of which show shorter Am—X than Eu—X distances for soft-donor X ligands.

Computational efforts have also been applied towards a description of lanthanide/actinide selectivity with phosphinic acid ligands. Shortly after reports of a high Am(III)/Eu(III) separation factor with Cyanex-301 were obtained,[2] experimental enthalpies and entropies of extraction from acidic aqueous solution with Cyanex-301 in kerosene (i.e., ΔH = 4.32 kcal/mol for Am and 10.43 kcal/mol for Eu; ΔS = -20.82 cal/(mol K) for Am and -15.71 cal/(mol K) for Eu) were determined.[3] Experimental separation factors of several other thiophosphinic acids are also reported in a relevant review by Bessen et al.[26] Prompted by empirical results, theorists began to work towards reaction energies which could be used to predict selectivity for separation with thiophosphinic acid ligands. Early works[13,15,19] exhibit the difficulty in predicting binding and extraction energies due to considerable solvent effects, where the computational results can be regarded as qualitative at best. Though such calculations may provide insight towards the prediction of selectivity of a particular ligand, a compensation of errors is expected when simultaneously comparing the relative selectivities of two similar ligands with the same approach. For example, Keith and Batista,[27] in their BP86 SC ECP study of trifluoromethylphenyl dithiophosphinic acids, found that the treatment of the solvent environment itself can result in differences in selectivity results. A polarizable continuum model reveals greater selectivity for Eu(III), while solvent environments

described with first principles or semi-empirical approaches show greater selectivity for Am(III). Importantly, however, when two ligands were compared using the same solvation approach, selectivity differences are identical, regardless of the description of the solvent.

Kaneko et al.[20, 21] extended previous work[13] on $M(Me_2PS_2)_3$ complexes by determining free energies of complex formation in both gas and implicit water solvent using an SC ECP approach with additional density functionals, now with varying E_X^{HF} contributions. They found that, regardless of the solvation environment, the BP86 functional, with 0% E_X^{HF}, erroneously predicts stronger complexation for M=Eu, while those functionals with greater E_X^{HF} admixtures, i.e., B3LYP (20%) and B2PLYP (54%), result in stronger complexation free energies for M=Am. The B2PLYP double-hybrid functional, which not only incorporates a greater exact-exchange admixture, but also MP2-like correlation using DFT-based molecular orbitals and energies, performed the best of the three functionals both in the gas phase and in implicit water solvent. In subsequent work, Kaneko et al.[22] expanded the selectivity calculations to a series of chalcogen-donating $N(XPMe_2)_2^-$ ligands. Their B2PLYP all-electron results for 3:1 complexes in implicit water solvent reveal that soft-donor ligands (i.e., X=S, Se, and Te) are much more selective for Am(III) over Eu(III) than hard-donor ligands (X=O); however, similar selectivity is seen across soft-donor ligands, with X=S and Se ligands being slightly more selective than X=Te ligands. In 2019, Pu et al.[23] enlisted B3LYP/SC ECP calculations in implicit solvent for multiple aryl dithiophosphinic acids, finding qualitative agreement with experiment in ranking the Eu/Am extraction selectivity of the three ligands considered, which differed by degree of trifluoromethyl substitution on the aryl rings. Finally, in 2019, Wang et al.[24] used M06-2X (56% E_X^{HF}) SC ECP calculations in implicit aqueous solvent to show greater Am(III) over Eu(III) selectivity by the model $Me_2PS_2^-$ ligand.

With deficiencies of description of complex structure and variability in predicting selectivity comes varying interpretation of metal—ligand bonding. Techniques including charge and spin population analyses,[10, 11, 13-15, 20-22, 24] overlap and density of states analyses, [10, 20-22,28], molecular orbital calculations,[10, 11, 24, 28, 29] x-ray spectra simulations,[29] and energy decomposition analysis[17, 19, 28] have been used to explain theoretical findings of Am— and Eu—soft-donor distances. Works by Kaneko et al.[20, 22] point to differences in contributions of f-orbitals to metal—ligand bonding, with a nonbonding contribution to Eu—S bonds and bond overlap in Am—S. Some studies also implicate metal d and s orbitals,[11, 28] while others[20, 22] show a similar contribution of f and d-orbitals to bonding in Am(III) and Eu(III) complexes. Differences in ionic character of the complexed metal cation, resulting from ligand-to-metal charge transfer have also been discussed using a second order perturbative approach.[11, 13, 28] With varying accounts of electronic contributions to bonding in trivalent f-block—phosphinic acid complexes, it is clear that a straightforward elucidation has yet to be obtained.

With the growing body of theoretical research, some questions remain unanswered pertaining to the validity and practical application of computational approaches towards an understanding and predicting Ln(III)/An(III) selectivity with soft-donor phosphinic acid ligands. First, what are the structures of Ln(III)— and An(III)—soft-donor complexes, specifically pertaining to metal—donor-atom distance? Second, which density functional approaches are the best in describing these separation processes, considering both complex structure and selectivity? In particular, unbalanced description of the "hard" ligands containing O donor atoms and "soft" ligands containing S or heavier donor atoms will lead to a bias in the predicted absolute and relative selectivities. Finally, how is metal—ligand binding in these complexes described with different density functionals, and how does this description explain selectivity results? To address these points, we begin with a post-Hartree-Fock study of model chalcogen-donor ligand complexes, resulting in both structures and relative selectivities. Using all-electron coupled cluster CCSD(T) calculations[30, 31] with the third-order scalar relativistic Douglas-Kroll-Hess Hamiltonian[32-34] at the extrapolated complete basis set limit as benchmark, we will assess the performance of several density functionals in predicting selectivity. Additionally, we appraise the extent to which descriptions of core electrons and electron correlation in our calculations affect selectivity results. Finally, we enlist a natural bond orbital analysis to compare metal—soft-atom bonding in Ln(III) and An(III) species, as described by different flavours of density functionals in order to relate differences in these descriptions to structural features and relative selectivities. We anticipate that insights and recommendations arising from the present work will lead concomitantly to more accurate and resource-conscious descriptions of ligand binding and selectivity of Ln(III)/An(III) separation with soft-donor ligands in future theoretical undertakings.

Computational Methods

Model homoleptic 3:1 complexes of H_2PX_2:Eu/Am, with X=O, S, Se, and Te were constructed to directly relate selectivities to electronic effects associated with ligand–metal ion interactions. The structures of all complexes were optimized using the ORCA quantum chemistry suite of software,[35-37] version 4.2.1, unless otherwise noted. Prior to optimization, all input structures were subject to self-consistent-field stability analyses, resulting in stable wavefunctions. Geometry optimizations enlisted unrestricted Hartree-Fock (UHF) or Kohn-Sham methods, with the aug-cc-pVTZ basis set for H, P, O, and S atoms,[38-40] and the SK-MCDHF-RSC/aug-cc-pVTZ-PP pseudopotential[41]/basis-set pair[41] for Te. The aug-cc-pVTZ basis set[42] was used for Se without a pseudopotential in geometry optimizations; however, single-point energy calculations were performed on optimized Se aug-cc-pVTZ structures in which SK-MCDHF-RSC/aug-cc-pVTZ-PP was instead used for Se,[41] resulting in small reaction energy differences (i.e., 0.03 kcal/mol for B3LYP, 0.05 for MP2) compared to those without a pseudopotential on Se. For Eu and Am, the treatment of 4f and 5f electrons, respectively, were considered both explicitly as valence electrons and implicitly as core electrons. For all small-core (SC ECP) f-in-valence calculations, the quasi-relativistic ECP28MWB/ECP28MWB_ANO and ECP60MWB/ECP60MWB_ANO effective-core-potential (RECP)/basis-set pairs (denoted SC-ANO below) developed by Dolg, Cao, and co-workers[43-48] were implemented for Eu(III) and Am(III), respectively, and all complexes were treated as charge-neutral septets. For all large-core (LC ECP) f-in-core calculations, all complexes were treated, using the Gaussian 16 suite of software,[49] as charge-neutral pseudosinglet species, and the ECP52MWB and ECP84MWB pseudopotentials were

respectively used for Eu(III) and Am(III) with the associated largest basis sets available.[50-52]

Optimizations of UHF-MP2 structures implemented resolution-of-identity[53-56] (RI) and the combined split-RI-J and "chain of spheres" COSX (RIJCOSX) approximations.[57] All RI calculations included auxiliary aug-cc-pVTZ/C basis sets for nonmetal atoms excepting Te,[58] and the SK-MCDHF-RSC/aug-cc-pVTZ-PP/C pair for Te.[59] RIJCOSX calculations included aug-cc-pVTZ/JK auxiliary basis sets for all nonmetal atoms excepting Te.[60] For Eu and Am, and for Te (RIJCOSX only), no suitable auxiliary basis sets were available; thus, the AutoAux feature in ORCA was engaged to generate auxiliary basis sets on the fly.[61]

Optimized RI-MP2/RIJCOSX geometries were subsequently used for single-point restricted open-shell-Hartree-Fock (ROHF), UHF, MP2 (without the RI or RIJCOSX approximations), and CCSD(T) single-point calculations, as implemented in the MOLPRO quantum chemistry software package.[30,31] UHF RI-MP2 single-point calculations were performed without the RIJCOSX approximation, using the ORCA suite of software.[35-37] For single-point MP2 SC ECP calculations, the Cao and Dolg basis sets were used as above, along with the aug-cc-pVnZ (n=D, T, Q) basis sets for H, P, O, and S atoms, and the SK-MCDHF-RSC/aug-cc-pVnZ-PP pseudopotential/basis-set combination for Se and Te. All-electron MP2 and CCSD(T) single-point calculations implemented the third-order scalar relativistic Douglas-Kroll-Hess (DKH3) Hamiltonian[32-34] and the cc-pVnZ-DK3 basis sets for Eu and Am,[62, 63] cc-pVnZ-DK for H, cc-pV(n+d)Z-DK for P, aug-cc-pVnZ-DK for O, Se, and Te, and aug-cc-pV(n+d)Z-DK for S.[38-40, 64, 65] For the sake of textual brevity, these all-electron basis sets will be collectively referred to as aVnZ-DK (n=D, T, Q) throughout this work. To best ensure the stability of all-electron DKH3 wavefunctions, multiple electron configurations were calculated for each species, differing by the specific occupation of the seven valence-f orbitals with the six f-electrons in Eu(III) or Am(III). Of all tested electron configurations for each species, that with the lowest energy was used in the consideration of the reaction energy.

The PBE (pure-GGA),[66] B3LYP (GGA-hybrid),[67] M06 (meta-hybrid-GGA),[25] wB97X (range-separated-hybrid),[68] and B2PLYP (double-hybrid)[69] functionals were directly implemented through the ORCA suite of software, while the B5050LYP[70] and PBE50[71] hybrid-GGA functionals were called in ORCA via the Libxc library of functionals.[67] B2PLYP geometry optimization calculations implemented both RI and RIJCOSX approximations with requisite auxiliary basis sets as described above, and subsequent single-point RI-B2PLYP energies calculated without the RIJCOSX approximation were used to determine the reaction energies reported in this work. All-electron B3LYP single-point calculations enlisted the second-order scalar relativistic Douglas-Kroll-Hess (DKH2) Hamiltonian[32, 33] with the SARC-DKH-TZVPP basis sets for Eu[72] and Am,[73] and the aug-cc-pVTZ-DK basis sets for nonmetal atoms.[38-40, 42, 64, 74] Focusing on a description of differential metal—ligand bonding, our calculations did not include any thermal or zero-point corrections to the reaction energies. However, frequency calculations were performed at the B5050LYP/LC ECP/aug-cc-pVTZ level for all species to ensure that the optimized structures are true minima.

Natural bond orbital (NBO) analyses of the wavefunctions were performed using the NBO7.0 program.[75] A combination of conventional natural population analysis,[76] Wiberg bond indices,[77] and perturbative treatment of donor–acceptor orbital interactions[78] was used to describe chemical bonding in the considered complexes.

Results and Discussion

Benchmarking Structure and Selectivity with Post-Hartree Fock Methods

Schematic structures of homoleptic 3:1 dichalcogen-phosphinic acid:Eu/Am complexes, $M(H_2PX_2)_3$, with M=Eu or Am, and X=O, S, Se, or Te are exemplified in Figure 1 along with the 3:1 Cyanex-301:metal complex. Complete spatial coordinates for all optimized geometries in this work are provided in the Supporting Information (SI). We acknowledge experimental structures which show that O-donating phosphinic acid ligands predominantly bind in a monodentate fashion to f-block metals, while S-donating ligands undergo bidentate coordination.[79] However, bidentate binding for all complexes was considered in order to allow for high-level benchmark calculations. Further, though both 3:1 and 4:1 complexes have been reported for S-donor ligands,[4, 5] we intentionally consider herein only 3:1 ligands with zero charge to minimize solvent effects, allowing us to focus on the differences in electronic effects across complexes. Model $H_2PX_2^-$ ligands were chosen as truncated analogues to alkylated phosphinic acid ligands both in consideration of computational expense and of previous works which note the role of interligand and ligand-solvent steric effects on selectivity.[13, 27] By choosing a small ligand, we hope to circumvent such steric effects, allowing us to focus on the role of ligand binding on structure and relative selectivity.

Average interatomic RI-MP2 SC ECP M—X distances are provided as the first entry in Table 1. For all species, shorter average interatomic distances are revealed for Eu(III) than for Am(III) complexes, in contrast to most previous SC ECP DFT results,[13, 14, 20-23, 28, 80] yet in agreement with previous Hartree-Fock and MP2 results[14] for soft-donor ligands. Most importantly, the present MP2 SC ECP M—S interatomic distance trends agree with previous experimental X-ray adsorption fine structure results for Cyanex-301 ligands[4, 5]

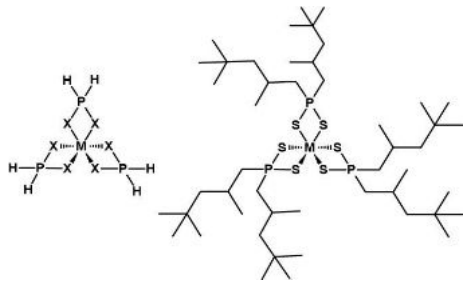

Figure 1: Schematic structures of 3:1 ligand—metal complexes used in this study (left) and for Cyanex-301 (right). M = Eu, Am; X = O, S, Se, Te.

To probe the selectivity of soft-donor dichalcogen-phosphinic acid ligands in the separation of Am(III) from Eu(III), we consider the energies of the reaction shown in Eq. 1:

$$Am(H_2PO_2)_3 + Eu(H_2PX_2)_3 \rightarrow Am(H_2PX_2)_3 + Eu(H_2PO_2)_3 \quad (1)$$

where X=S, Se, or Te. In this manner, we compare the relative selectivity of each ligand with respect to its phosphinic acid (X = O) analogue. By comparing the selectivities of two ligands at a time, we expect to avoid large errors that may result from solvation effects for charged complexes, which strongly depend on the description of a

solvation environment, as noted previously.[27] All-electron MP2 reaction energies for these reactions are provided in Table 2, and as solid circles in Figure 2. All energies provided are the result of single-point calculations at the RI-MP2/SC-ANO/aug-cc-pVTZ geometries reflected in Table 1. Negative reaction energies for all X-donor

Table 1: RI-MP2/SC-ANO/aug-cc-pVTZ and DFT/SC-ANO and LC/aug-cc-pVTZ average M—X interatomic distances of $M(H_2PX_2)_3$ complexes, in Angstroms.

	X=O	X=S	X=Se	X=Te
RI-MP2/SC ECP				
$Eu(H_2PX_2)_3$	2.347	2.752	2.869	3.068
$Am(H_2PX_2)_3$	2.392	2.784	2.896	3.095
d(Am—X) – d(Eu—X)	0.045	0.032	0.027	0.027
B3LYP/SC ECP				
$Eu(H_2PX_2)_3$	2.384	2.862	3.016	3.275
$Am(H_2PX_2)_3$	2.426	2.867	3.004	3.228
d(Am—X) – d(Eu—X)	0.042	0.005	-0.012	-0.047
PBE/SC ECP				
$Eu(H_2PX_2)_3$	2.402	2.862	3.005	3.224
$Am(H_2PX_2)_3$	2.415	2.832	2.967	3.181
d(Am—X) – d(Eu—X)	0.013	-0.030	-0.038	-0.043
M06/SC ECP				
$Eu(H_2PX_2)_3$	2.356	2.805	2.931	3.278
$Am(H_2PX_2)_3$	2.399	2.816	2.935	3.167
d(Am—X) – d(Eu—X)	0.043	0.011	0.004	-0.111
wB97X/SC ECP				
$Eu(H_2PX_2)_3$	2.374	2.811	2.951	3.194
$Am(H_2PX_2)_3$	2.419	2.840	2.974	3.193
d(Am—X) – d(Eu—X)	0.045	0.029	0.023	-0.001
B5050LYP/SC ECP				
$Eu(H_2PX_2)_3$	2.366	2.824	2.953	3.175
$Am(H_2PX_2)_3$	2.413	2.858	2.986	3.207
d(Am—X) – d(Eu—X)	0.047	0.034	0.033	0.032
PBE50/SC ECP				
$Eu(H_2PX_2)_3$	2.350	2.794	2.923	3.132
$Am(H_2PX_2)_3$	2.394	2.823	2.951	3.157
d(Am—X) – d(Eu—X)	0.044	0.029	0.028	0.025
B2PLYP/SC ECP				
$Eu(H_2PX_2)_3$	2.366	2.804	2.916	3.120
$Am(H_2PX_2)_3$	2.413	2.836	2.943	3.145
d(Am—X) – d(Eu—X)	0.047	0.032	0.027	0.025
B3LYP/LC ECP				
$Eu(H_2PX_2)_3$	2.398	2.858	2.993	3.209
$Am(H_2PX_2)_3$	2.463	2.920	3.054	3.272
d(Am—X) – d(Eu—X)	0.065	0.062	0.061	0.063
B5050LYP/LC ECP				
$Eu(H_2PX_2)_3$	2.402	2.875	3.014	3.239
$Am(H_2PX_2)_3$	2.467	2.935	3.074	3.299
d(Am—X) – d(Eu—X)	0.065	0.060	0.060	0.060

complexes reveal more favorable Am(III) over Eu(III) selectivity with these soft ligands than with the hard O-donor ligand. Further, all reactions show reasonable convergence with respect to the size of the X-containing-species basis set at triple-zeta energies, which differ from those of the extrapolated complete basis set limit (CBS)[81,82] by 0.68, 0.67, and 0.97 kcal/mol for X=S, Se, and Te, respectively. Quadruple-zeta energies result in lower respective differences: 0.25, 0.25, and 0.36 kcal/mol, albeit at a significant increase in computational expense. Post-double-zeta reaction energies indicate a selectivity trend of Te > Se > S >> O.

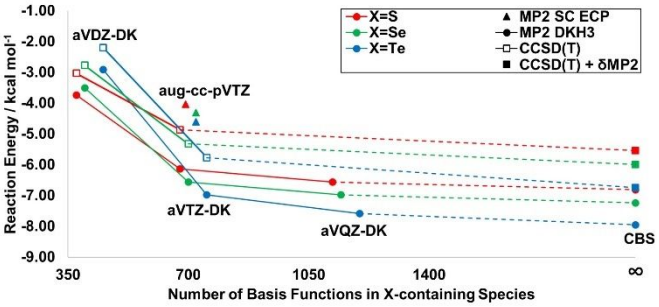

Figure 2: ROHF MP2 and CCSD(T) reaction energies, in kcal/mol, for $Am(H_2PO_2)_3$ + $Eu(H_2PX_2)_3$ → $Am(H_2PX_2)_3$ + $Eu(H_2PO_2)_3$. In the figure, ligand complexes are indicated with colors and computational approaches are indicated with symbol shapes.

All-electron CCSD(T)-DKH3 single-point energies, provided in Table 2 and as open squares in Figure 2, show similar differences as all-electron MP2-DKH3 reaction energies moving from double- to triple-zeta calculations. Thus, we assume that convergence behaviour to the complete-basis-set limit will be similar for CCSD(T) as for MP2. With this assumption, we estimate the extrapolated CCSD(T) energies with a composite scheme, as follows:

$$E(CCSD(T) + \delta MP2) = E(CCSD(T/aVTZ\text{-}DK) - E(MP2/aVTZ\text{-}DK) + E(MP2/CBS) \quad (2)$$

Composite CCSD(T) + δMP2 reaction energies are provided in Figure 2 (solid squares) and Table 2. CCSD(T) reaction energies are systematically lower in magnitude (by 1.21 to 1.27 kcal/mol at the triple-zeta and composite/CBS levels) than MP2 reaction energies and closer to HF/aVTZ-DK values (i.e., -4.13 kcal/mol for X=S; -3.75 kcal/mol for X=Se, and -5.28 kcal/mol for X=Te). This is expected, considering the well-known tendency for MP2 methods to overcorrelate electrons. Results from extraction experiments show that Cyanex-301 has an Am/Eu extraction Gibbs' free energy 5.43-6.83 kcal/mol lower than that of the O-donor analogue Cyanex-272.[3, 20, 79, 83] This is in a very good agreement with our best estimate using the composite CCSD(T) + δMP2 scheme (i.e., 5.54 kcal/mol), given a model reaction with simplified complex stoichiometry and truncated ligands.

Table 2: ROHF MP2 and ROCCSD(T) reaction energies, in kcal/mol, for $Am(H_2PO_2)_3$ + $Eu(H_2PX_2)_3$ → $Am(H_2PX_2)_3$ + $Eu(H_2PO_2)_3$.[a]

	MP2 SC ECP[b]	MP2 DKH3	CCSD(T) DKH3	CCSD(T)+δMP2
X=S				
aVDZ-DK	--	-3.75	-3.03	--
aVTZ-DK	-4.03	-6.13	-4.87	--
aVQZ-DK	--	-6.56	--	--
CBS	--	-6.81	--	-5.54
X=Se				
aVDZ-DK	--	-3.51	-2.77	--
aVTZ-DK	-4.32	-6.56	-5.32	--
aVQZ-DK	--	-6.98	--	--
CBS	--	-7.23	--	-5.99
X=Te				
aVDZ-DK	--	-2.91	-2.20	--
aVTZ-DK	-4.60	-6.98	-5.77	--
aVQZ-DK	--	-7.59	--	--
CBS	--	-7.95	--	-6.74

[a]See the Computational Methods section of text for a description of basis set abbreviations. [b]MP2/SC-ANO/aug-cc-pVnZ calculations.

With an understanding of energy differences between all-electron MP2 and CCSD(T) results, we proceed to investigate the role of implicit treatment of core electrons on descriptions of selectivity. Single-point MP2 SC ECP energies of all structures are provided in Table 2 and as triangles in Figure 1. We find a systematic decrease in the magnitude of the triple-zeta reaction energies relative to all-electron MP2-DKH3/aVTZ-DK results (i.e., 2.10, 2.24, and 2.38 kcal/mol reaction energy differences for X=S, Se, and Te, respectively). The main source of the differences arises from using a pseudopotential and its accompanied basis set (SC-ANO) versus an all-electron relativistic description of the core electrons for Eu and Am. Other differences involve the use of aug-cc-pVnZ-PP for Se and Te instead of aug-cc-pVnZ-DK, as well as not using diffuse functions on H or P in the all-electron calculations. In addition, tight d functions were added on P and S in the all-electron calculations, but this was found to only affect the reaction enthalpies by under 0.1 kcal/mol. To approximately decouple the discrepancies due to the ECP from those of their basis sets, pseudopotential MP2 calculations were performed by employing approximate cc-pVTZ-PP basis sets on Eu and Am that are equivalent to the all-electron cc-pVTZ-DK3 sets. These PP basis sets on Eu and Am, provided in the SI, were constructed by re-contracting the cc-pVTZ-DK3 sets in the presence of the ECPs using the same procedures as outlined in Refs. 63 and 63. The same basis sets as described above in the SC-ANO PP calculations were used on the other atoms. These new PP calculations now yielded reaction enthalpies larger in magnitude than the corresponding all-electron results by just 0.55, 0.65, and 0.72 kcal/mol for X=S, Se, and Te, respectively, which are in much better agreement compared to using the SC-ANO basis sets.

Table 3: MP2 reaction energies, in kcal/mol, for $Am(H_2PO_2)_3 + Eu(H_2PX_2)_3 \rightarrow Am(H_2PX_2)_3 + Eu(H_2PO_2)_3$, for various numbers of correlated electrons.

Finding similar trends in relative selectivity between the two ligands (Eq. 1) for MP2 approaches regardless of whether core electrons are treated explicitly (i.e., an all-electron approach) or implicitly (i.e., a small-core pseudopotential approach), we are meaningfully able to validate aspects of our global treatment using the less computationally intensive SC ECP approach. We also find that a restricted open-shell approach yields similar reaction energies as an unrestricted approach, with a difference of no more than 0.03 kcal/mol for any reaction (SI).

UHF RI-MP2 SC ECP	n=D	n=T	n=Q	CBS
X=S				
aug-cc-pVnZ 74 (s,p,f) correlated electrons	-4.24	-4.30	--	--
aug-cc-pVnZ 84 (s,p,d,f) correlated electrons	-5.46	-5.36	--	--
aug-cc-pwCVnZ 84 (s,p,d,f) correlated electrons	-4.46	-4.74	--	--
X=Se				
aug-cc-pVnZ 74 (s,p,f) correlated electrons	-5.07	-4.74	--	--
aug-cc-pVnZ 144 (s,p,d,f) correlated electrons	-6.63	-5.84	--	--
aug-cc-pwCVnZ 144 (s,p,d,f) correlated electrons	-5.45	-5.52	--	--
X=Te				
aug-cc-pVnZ 74 (s,p,f) correlated electrons	-6.09	-4.77	--	--
aug-cc-pVnZ 144 (s,p,d,f) correlated electrons	-7.65	-6.16	--	--
aug-cc-pwCVnZ 144 (s,p,d,f) correlated electrons	-6.29	-5.46	--	--
ROHF MP2 DKH3	**n=D**	**n=T**	**n=Q**	**CBS**
X=Te				
awCVnZ-DK 74 (s,p,f) correlated electrons	--	-6.33	-7.51	-8.16
awCVnZ-DK 92 (s,p,d,f) correlated electrons	--	-6.88	-7.84	-8.36

We also probed the effect that the extent of electron correlation had on reaction energies resulting from MP2 SC ECP calculations. A comparison of the results from which only valence s-, p-, and f-electrons are correlated to those in which outer d-electrons are correlated as well provides insight into the role of d-electron correlation on reaction selectivity at the MP2 level. Reaction energies calculated up to this point in our discussion involve the treatment of the following electrons as valence: H 1s; O 2s2p; P, S 3s3p; Se 4s4p; Te 5s5p; Eu 5s5p6s4f; Am 6s6p7s5f; for a total of 74 correlated electrons for all reactive complexes. Our choice to correlate only s, p, and f electrons reflects our choice of the standard basis sets,[44, 45, 47, 48] which were not designed to include d-electron correlation. In fact, as Table 3 shows, substantial increases in the magnitude of the reaction energies (e.g., by 1.06, 1.10, and 1.39 kcal/mol for the X=S, Se, and Te reactions, respectively, calculated with n=T basis sets) were obtained when d-electrons were also correlated within this approach. However, by employing the appropriate core-valence aug-cc-pwCVTZ basis sets for light elements[84] and augmenting Dolg and Cao RECP basis sets for Eu(III) and Am(III) with outer core s, p, d, f, and g basis functions for Eu and Am (SI) taken from all-electron cc-pwCVTZ-DK3 basis sets,[84] we are able to better account for d-electron correlation. Thus, in a separate set of calculations, we used these alternate basis sets and correlated outer d-electrons in Se, Te, Eu and Am, for a total of 84 correlated electrons in X=O and S complexes and 144 correlated electrons in X=Se and Te species. The resulting reaction energies are provided in Table 3 and reveal similar reaction energies (e.g., within 0.44, 0.78, and 0.69 kcal/mol for the X=S, Se, and Te reactions, respectively at the n=T level) as treatments without d-electron correlation. We also find similar results across all-electron calculations, also presented in Table 3 for the X=Te reaction, wherein we compare the results of correlating 74 electrons in each species as described for pseudopotential calculations with those in which 4/5s, 4/5p, and 4/5d electrons were additionally correlated for Eu/Am, for a total of 92 correlated electrons in each complex. The correlation of the outer core electrons does not substantially alter the reaction energies, with differences ranging from 0.55 to 0.20 kcal/mol at the triple-zeta level and CBS limit, respectively, suggesting that the correlation of these electrons do not play a significant role in Eu/Am selectivity by dichalcogen-phosphinic acid ligands. These results also highlight the necessity to choose basis sets specifically designed to describe core-valence excitations. We finally note that the RI-MP2/SC ECP results in Table 3 do not reflect a true basis set dependence within aug-cc-pVnZ (n= D,T), since the basis sets on Eu (ECP28MWB_ANO) and Am (ECP60MWB_ANO) are fixed in these calculations.

Evaluating Density Functionals for Prediction of Metal-ligand Bond Distances and Relative Selectivity

DFT Structures of Eu/Am(H_2PX_2)$_3$ Complexes. Our exploration of post-Hartree-Fock approaches to probe the relative selectivities of chalcogen-containing phosphinic acid ligands in the separation of lanthanides and actinides leaves us with an excellent set of benchmarks by which to evaluate a variety of DFT methods for efficient calculations of selectivity. From Table 1, we remind the reader that for all X-containing species, Am—X interatomic distances are longer than Eu—X distances, as optimized with a small-core RI-MP2 SC ECP approach. Additionally, we find that the difference between Am—X and Eu—X distances decreases with progression down the chalcogen group, with average Am—O distance 0.045 Å longer than Eu—O, continuing to 0.032 Å for X=S, and 0.027 Å for X=Se and X=Te, which is consistent with the experimental bond distances for the related complexes. [4-7, 9, 10] Therefore, we are confident to use trends in MP2 distances by which to evaluate various DFT methods.

Table 1 shows interatomic distances resulting from geometries optimized with a plethora of DFT methods, including the pure-GGA PBE functional, the GGA-hybrid B3LYP, B5050LYP and PBE50 functionals, the meta-hybrid-GGA M06 functional, the range-separated-hybrid wB97X functional, and the double-hybrid B2PLYP functional (full sets of optimized coordinates are available in the SI). Herein, either SC ECP or LC ECP descriptions were used for metal atoms, and the aug-cc-pVTZ basis set (H, P, O, S, Se) or the SK-MCDHF-RSC/aug-cc-pVTZ-PP pseudopotential/basis-set pair (Te) were enlisted for nonmetals, as described in the Computational Methods section.

Table 1 shows that SC ECP calculations with many commonly used density functionals result in striking differences in interatomic distances from MP2 distances. While MP2 results show substantially shorter Eu—X than Am—X distances for all X tested, three of these functionals—B3LYP, PBE, and M06—show similar or shorter Am—S distances in comparison to Eu—S distances.

Beyond X=S, longer Eu—X than Am—X distances result for structures optimized with these density functionals, as well as with wB97X, for at least one soft-donor complex. B3LYP shows longer Eu—X than Am—X distances for X=Se and Te. PBE reveals longer average Eu—X distances for X=Se and Te, along with S. M06 and wB97X show longer Eu—Te than Am—Te. Notably, all functionals resulting in shorter Am—X distances employ a relatively small admixture of Hartree-Fock exchange, E_X^{HF}. PBE, incorporating no exact exchange, is the worst performing of the functionals tested for predicting the trends in interatomic distances. This is followed by B3LYP with a 20% E_X^{HF} admixture, and subsequently wB97X, with 16% E_X^{HF}, and M06, with 27% E_X^{HF}. A ranking of E_X^{HF} for these functionals correlates with performance in reproducing MP2 distance trends, save for wB97X, which has a lower E_X^{HF} admixture than B3LYP, yet shows a better M—Se distance difference. As wB97X is a range-separated hybrid, with 16% E_X^{HF} at short range and, uniquely amongst the functionals tested, 100% E_X^{HF} at long range, we note the contribution of long-range exchange towards the correct prediction of structure in these complexes. Those functionals with larger fractions of exact exchange, namely the B5050LYP (i.e., 50% E_X^{HF}) and PBE50 (50% E_X^{HF}) hybrid functionals and the B2PLYP (53% E_X^{HF}) double-hybrid functional, result in longer average Am—X than Eu—X for all X, in agreement with the MP2 results. Our finding that more accurate trends in bond distances result from density functionals with larger fractions of Hartree-Fock exchange is in line with previous work by Pu[23] and Wang[24] and recommendations by Dolg et al.[14]

Finally, an LC ECP description of the lanthanide/actinide center overcorrects erroneous trends in Eu—X and Am—X distances seen from SC ECP results. For B3LYP, greater Am—X than Eu—X distances are now shown for X=Se and X=Te, though these differences in distance are overestimated with respect to RI-MP2 SC ECP results. B5050LYP calculations, which revealed correct, yet slightly overestimated distance trends with SC ECP, overestimate all distance trends even more with the LC ECP approach. This overestimation of differences in distances relative to MP2 SC ECP reflects an uneven lengthening of Am—X bonds in relation to Eu—X when applying an LC ECP approach. Taking the LC ECP results of both B3LYP and B5050PYLP into consideration, we recommend an SC ECP approach with high E_X^{HF} to describing structures of Eu/Am—phosphinic acid complexes.

DFT Reaction Energies and Relative Selectivities. Energies of reaction (Eq. 1) resulting from DFT calculations are provided in Table 4 and Figure 3. For the sake of comparison, CCSD(T) + δMP2 composite DKH3 all-electron energies (Table 2) are also shown (solid black triangles) in the figure. We find that the best agreement with CCSD(T) + δMP2 energies results from small-core B5050LYP (solid blue circles), PBE50 (solid purple circles), and B2PLYP (solid brown circles), all of which reveal a decreasing trend in reaction energies, indicating an increasing trend in relative Ln/An selectivity, progressing down the chalcogen group. All three functionals reveal similar energies to composite results in all reactions. Of these, the first two functionals slightly overestimate reaction energies (underestimating selectivity) at all points, with average deviations of 0.29 ± 0.21 kcal/mol (B5050LYP/SC ECP) and 0.37 ± 0.04 kcal/mol (PBE50) from composite. The third, and the only double-hybrid functional, B2PLYP, underestimates the energies of all three reactions, with an average deviation of -0.33 ± 0.06 kcal/mol. These three DFT methods include large fractions of exact exchange, also yielding the best performance in predicting changes in the bond distances (vide supra). Conversely, functionals that incorporate a smaller admixture of exact exchange show worse performance in predicting selectivity than those with larger admixtures. In contrast

Table 4: DFT reaction energies, in kcal/mol, for $Am(H_2PO_2)_3 + Eu(H_2PX_2)_3 \rightarrow Am(H_2PX_2)_3 + Eu(H_2PO_2)_3$ obtained with several flavours of density functionals and different treatment of f and inner electrons.

	X=S	X=Se	X=Te
B3LYP/DKH2[a]	-2.19	-0.96	2.00
B3LYP/DKH2[b]	-3.73	-2.53	-0.53
B3LYP/SC ECP	-2.38	-0.90	3.01
PBE/SC ECP	1.00	3.36	6.78
M06/SC ECP	-1.86	0.07	13.65
wB97X/SC ECP	-3.22	-3.00	-0.67
B5050LYP/SC ECP	-5.01	-5.78	-6.60
PBE50/SC ECP	-5.14	-5.66	-6.36
B2PLYP/SC ECP	-5.82	-6.31	-7.14
B3LYP/LC ECP	-3.96	-5.09	-6.44
B5050LYP/SC ECP[c]	-4.88	-6.20	-7.21

[a]Single-point energy at optimized B3LYP/SC ECP/aug-cc-pVTZ geometry.
[b]Single-point energy at optimized MP2/SC ECP/aug-cc-pVTZ geometry.
[c]Single-point energy at optimized PBE/SC ECP/aug-cc-pVTZ geometry.

to CCSD(T) + δMP2 reaction energies, those resulting from SC ECP calculations with the B3LYP (solid red circles in Figure 3), PBE (solid orange circles), M06 (solid light green circles), and wB97x (solid dark green circles) functionals show an increase when moving down the

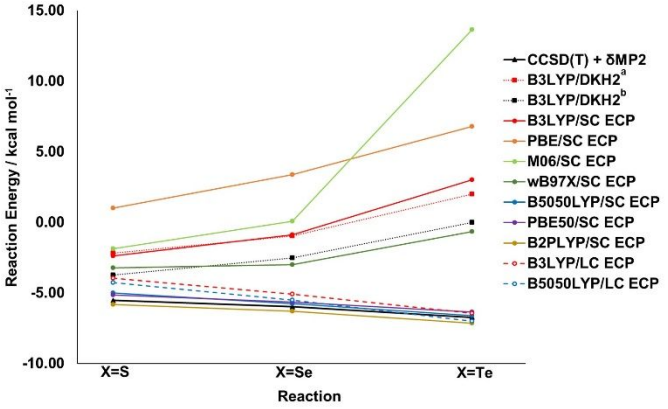

Figure 3: DFT reaction energies, in kcal/mol, for $Am(H_2PO_2)_3 + Eu(H_2PX_2)_3 \rightarrow Am(H_2PX_2)_3 + Eu(H_2PO_2)_3$ obtained with several flavours of density functionals and different treatments of f and inner-shell electrons. Composite CCSD(T) + δMP2 results (Table 2) are shown with solid triangles. Small-core DFT calculations are shown with solid circles, large-core with open circles, and single-point all-electron calculations with solid squares. [a]Single-point energy at optimized B3LYP/SC-ANO/aug-cc-pVTZ geometry. [b]Single-point energy at optimized RI-MP2/SC-ANO/aug-cc-pVTZ geometry.

chalcogen group from X=S to X=Te, yielding a qualitatively wrong trend. Moreover, the increase in energy is greater from the X=Se to X=Te than from the X=S to X=Se reactions for all these low-E_X^{HF} functionals. As a result of these trends, deviations from CCSD(T) + δMP2 reaction energies are both greater and less uniform from this selection of functionals (i.e., average deviation for B3LYP/SC ECP: 6.00 ± 3.39 kcal/mol, PBE: 9.80 ± 3.51 kcal/mol, M06: 10.04 ± 9.04 kcal/mol, wB97X: 3.79 ± 2.00 kcal/mol) than from those with larger E_X^{HF} admixtures.

A large-core description of outer f electrons shows an improvement in predicting selectivity over a small-core description for low-E_X^{HF} functionals and a diminishment over high-E_X^{HF} ones. As with the latter, a LC ECP treatment results in increasing selectivity (i.e., decreasing reaction energies) when moving down the periodic table from X=S to X=Te for both functionals considered, in agreement with composite CCSD(T)/MP2-DKH3 results. As such, B3LYP/LC ECP average deviations decrease to 0.93 ± 0.64 kcal/mol. However, for B5050LYP which already predicts a trend of increasing selectivity from S- to Te- donor ligands with SC ECP, deviations from CCSD(T) + δMP2 results increase in magnitude to 0.49 ± 0.77 kcal/mol and decrease in uniformity in comparison to small-core results.

Considering the enhanced performance in predicting selectivity by the small-exact-admixture B3LYP functional when a large-core description of Eu and Am is implemented, a question arises as to whether spurious trends in low-E_X^{HF}-DFT SC ECP reaction energies are due to the density functional itself or the particular ECP description of Ln(III) and An(III) implemented. In order to parse the particular influences of DFT from the core treatment of electrons, we have calculated B3LYP reaction energies with an all-electron DKH2 approach.[32, 33] These energies, calculated at the single point of optimized RI-MP2 SC ECP and B3LYP SC ECP structures, are presented in Table 4 and as closed squares in Figure 3: red at B3LYP geometries and black at RI-MP2 geometries. We find that, regardless of the geometry considered, a decrease in the magnitude of the reaction energy is revealed moving from X=S to X=Te with the B3LYP all-electron approach, in line with the B3LYP SC ECP trend. Thus, we find that the decrease in selectivity moving down the chalcogen group for these ligands as predicted with low-E_X^{HF} functionals is indeed due to the nature of the density functional and its inherent delocalization error, as pointed out by Dolg et al.[14] As B3LYP LC ECP calculations, wherein f-electrons are treated implicitly within the core, reveal the opposite trend, in agreement with CCSD(T) + δMP2 all-electron results, the explicit description of valence f-electrons for trivalent f-metal complexes with S, Se, and Te donor atoms using B3LYP SC ECP or any other DFT method with small E_X^{HF} is problematic and should be avoided.

To parse the role of the specific functional selected from that of the geometry of the complex, we have calculated B5050LYP/SC ECP selectivities at the PBE/SC ECP geometries. The resulting reaction energies, provided as the last entry in Table 4, are similar to the B5050LYP/SC ECP selectivities calculated at the optimized B5050LYP/SC ECP geometries. Thus, variations in complex geometries around the f-block-element core play a minor role in describing selectivities, in comparison to the significant role of the choice of a density functional.

We find that Hartree-Fock reaction energies show an increase in magnitude when moving from X=S to the X=Te reactions, with similar relative selectivities (for example, HF SC ECP/aug-cc-pVTZ reaction energies are -5.38 (X=S), -5.46 (X=Se), and -7.54 kcal/mol (X=Te). These values differ from respective MP2/aVTZ-DK energies by 0.75, 1.10, and 0.56 kcal/mol, and CCSD(T)/aVTZ-DK by -0.51, -0.14, and -1.76 kcal/mol) to MP2 and CCSD(T) results. This indicates that many-body correlation effects at the CCSD(T) level provide only a relatively small contribution to the reaction energy and most of the effects contributing to relative selectivity can be described based on a mean-field theory using one-electron approximation. Therefore, DFT methods will be suitable to investigate chemical bonding and the origin of selectivity with phosphinic acid ligands.

Natural Bond Orbital Analysis. Natural electron configurations, spin densities, charges and Wiberg bond indices (WBIs) calculated using two density functionals with different E_X^{HF} admixtures (B3LYP SC ECP/aug-cc-pVTZ and B5050LYP SC ECP/aug-cc-pVTZ) as well as HF SC ECP/aug-cc-pVTZ and MP2 SC ECP/aug-cc-pVTZ, are summarized in Table 5.

Understanding the nature of chemical bonding interactions between Eu(III)/Am(III) ions and the phosphinic acid ligands provides important insight into observed differences in the bond lengths and selectivities predicted by various computational methods explored in our study. According to the NBO analysis, the Eu/Am—X dative bonds originate from a characteristic σ-type donation of electron density from X (X=O, S, Se, Te) lone pair (LP) to the Eu/Am. Figure 4a shows the representative leading orbital interaction, stemming from an overlap of the O LP (8.64% s and 91.36% p-character) with an acceptor orbital of primarily 6d character on Am (14.56% s, 0.64% p, 66.20% d, 18.60% f). The resulting Am—O bond, which is mostly localized on O, is shown in Figure 4b. There are also back-bonding interactions of partially filled metal f orbitals with the ligands, which are more apparent for Am 5f orbitals compared to Eu 4f orbitals as

Table 5: NBO results for Eu/Am—phosphinic acid complexes.

Natural Electron Configuration of Metal Ion

	$Eu(H_2PO_2)_3$	$Eu(H_2PS_2)_3$	$Eu(H_2PSe_2)_3$	$Eu(H_2PTe_2)_3$	$Am(H_2PO_2)_3$	$Am(H_2PS_2)_3$	$Am(H_2PSe_2)_3$	$Am(H_2PTe_2)_3$
MP2	6s(0.14)	6s(0.36)	6s(0.42)	6s(0.53)	7s(0.16)	7s(0.40)	7s(0.45)	7s(0.52)
	4f(5.99)	4f(5.90)	4f(5.98)	4f(5.96)	5f(6.03)	5f(6.04)	5f(6.04)	5f(6.01)
	5d(0.76)	**5d(1.62)**	**5d(1.82)**	**5d(2.04)**	**6d(0.63)**	**6d(1.53)**	**6d(1.77)**	**6d(2.12)**
	6p(0.02)	6p(0.04)	6p(0.03)	6p(0.05)	7p(0.02)	7p(0.03)	7p(0.03)	7p(0.04)
	5f(0.03)	5f(0.04)	5f(0.04)	5f(0.04)				
	6d(0.11)	6d(0.12)	6d(0.11)	6d(0.10)				
HF	6s(0.11)	6s(0.33)	6s(0.38)	6s(0.47)	7s(0.12)	7s(0.35)	7s(0.41)	7s(0.47)
	4f(6.01)	4f(6.01)	4f(6.01)	4f(6.01)	5f(6.05)	5f(6.06)	5f(6.05)	5f(6.04)
	5d(0.54)	**5d(1.37)**	**5d(1.52)**	**5d(1.69)**	**6d(0.44)**	**6d(1.29)**	**6d(1.49)**	**6d(1.79)**
	6d(0.03)	6p(0.01)	6p(0.01)	6p(0.02)		7p(0.01)	7p(0.01)	7p(0.01)
		5f(0.01)	5f(0.01)	5f(0.01)				
		6d(0.04)	6d(0.04)	6d(0.03)				
B5050LYP	6s(0.12)	6s(0.35)	6s(0.40)	6s(0.49)	7s(0.13)	7s(0.38)	7s(0.44)	7s(0.52)
	4f(6.04)	4f(6.04)	4f(6.04)	4f(6.04)	5f(6.10)	5f(6.11)	5f(6.10)	5f(6.09)
	5d(0.60)	**5d(1.32)**	**5d(1.43)**	**5d(1.53)**	**6d(0.48)**	**6d(1.24)**	**6d(1.40)**	**6d(1.61)**
	6d(0.04)	6p(0.01)	6p(0.01)	6p(0.02)		7p(0.01)	7p(0.01)	7p(0.02)
		5f(0.01)	5f(0.01)	5f(0.01)				
		6d(0.04)	6d(0.03)	6d(0.02)				
B3LYP	6s(0.13)	6s(0.34)	6s(0.39)	6s(0.44)	7s(0.15)	7s(0.39)	7s(0.45)	7s(0.52)
	4f(6.12)	**4f(6.29)**	**4f(6.41)**	**4f(6.62)**	**5f(6.17)**	**5f(6.23)**	**5f(6.25)**	**5f(6.30)**
	5d(0.65)	5d(1.22)	5d(1.23)	5d(1.07)	6d(0.53)	6d(1.28)	6d(1.45)	6d(1.58)
	6d(0.04)	6p(0.01)	6p(0.01)	6p(0.01)		7p(0.01)	7p(0.01)	7p(0.01)
		5f(0.01)	6d(0.03)	6d(0.02)				
		6d(0.04)						

Natural Spin Density of Metal Ion

	$Eu(H_2PO_2)_3$	$Eu(H_2PS_2)_3$	$Eu(H_2PSe_2)_3$	$Eu(H_2PTe_2)_3$	$Am(H_2PO_2)_3$	$Am(H_2PS_2)_3$	$Am(H_2PSe_2)_3$	$Am(H_2PTe_2)_3$
MP2	6.026	5.991	6.102	6.124	5.994	6.078	6.104	6.171
HF	6.013	6.060	6.078	6.114	5.991	6.064	6.089	6.151
B5050LYP	6.018	6.075	6.094	6.126	5.988	6.070	6.098	6.144
B3LYP	6.067	6.327	6.468	6.708	5.999	6.135	6.196	6.329

Natural Charge of Metal Ion

	$Eu(H_2PO_2)_3$	$Eu(H_2PS_2)_3$	$Eu(H_2PSe_2)_3$	$Eu(H_2PTe_2)_3$	$Am(H_2PO_2)_3$	$Am(H_2PS_2)_3$	$Am(H_2PSe_2)_3$	$Am(H_2PTe_2)_3$
MP2	2.039	1.098	0.665	0.388	2.084	0.869	0.580	0.175
HF	2.301	1.232	1.035	0.781	2.358	1.227	0.971	0.627
B5050LYP	2.201	1.238	1.078	0.903	2.242	1.199	0.987	0.717
B3LYP	2.062	1.093	0.937	0.840	2.103	1.022	0.786	0.544

Wiberg Bond Index of M—X Bond

	$Eu(H_2PO_2)_3$	$Eu(H_2PS_2)_3$	$Eu(H_2PSe_2)_3$	$Eu(H_2PTe_2)_3$	$Am(H_2PO_2)_3$	$Am(H_2PS_2)_3$	$Am(H_2PSe_2)_3$	$Am(H_2PTe_2)_3$
MP2	0.240	0.490	0.520	0.571	0.237	0.502	0.553	0.613
HF	0.206	0.464	0.501	0.545	0.198	0.477	0.526	0.591
B5050LYP	0.234	0.466	0.499	0.534	0.230	0.486	0.530	0.581
B3LYP	0.273	0.498	0.518	0.489	0.269	0.530	0.578	0.623

can be judged from the calculated second-order stabilization energies $E^{(2)}$ in the SI (Table S2).

It is worth noting that in the $Am(H_2PTe_2)_3$ complex, the coordinative σ Am—Te bond (Figure 4c) becomes increasingly polarized toward the Am ion, because of the enhanced basicity of the ligand and hence more diffuse nature of its LPs, enabling stronger overlap with the acceptor orbitals. The progressive increased in strength of coordinative donations on going from O to Te donor atoms is also seen in the decreasing charge on the Am ion as a result of electron density transfer (Table 5). The WBIs are also much higher for the Am−Te bonds (0.613) than they are for the Am−O bonds (0.237) at the MP2 level of theory (Table 5). In addition, following the Am/Eu selectivity trends predicted by the MP2, WBI values are higher, and charge on the metal is lower for the Am complexes with S, Se, and Te donors compared to that of the corresponding Eu complexes.

The NBO results for the MP2, HF, B5050LYP and B3LYP wavefunctions, and in particular natural electron configurations of the Eu/Am ions in their respective complexes (Table 5) provide an explanation for the failure of the density functionals with low E_X^{HF} admixtures to correctly predict the bond lengths and selectivities,

which seem to be related to a somewhat different mechanism of the Eu/Am—X bond formation. While MP2, HF and B5050LYP natural electron configurations emphasize the importance of electron transfer to 7s and 6d Am (6s and 5d Eu) orbitals, B3LYP tends to overfill f orbitals both for Eu and Am along the O, S, Se, Te series and gives excessive spin densities in some cases. With selectivity in mind, we further find that B3LYP spin densities of Eu complexes are more deviant than those of analogous Am complexes, and deviation from MP2/HF/B5050LYP spin densities increases along the O, S, Se, Te series. Moreover, natural electron configurations across complexed Eu—X and Am—X species as calculated with MP2, HF, and B5050LYP are generally invariant throughout the chalcogen-donor complexes probed (e.g., 4f Eu and 5f Am occupations differ from one another by 0.04 electrons in O-donor complexes, and by 0.05 electrons in Te-donor complexes), while analogous B3LYP occupation differences decrease significantly across the series (from 0.05 to -0.32 electrons). This result supports the assertion by Dolg et al.[14] that low-E_X^{HF} functionals fail to describe the Eu(III) $4f^6$ shell correctly. Importantly, our B3LYP electron configurations also implicate the $5f^6$ shell in Am(III), albeit to a lesser degree. Additionally, as can be seen from Table 5, WBI obtained with B3LYP for the Eu—Te bond clearly falls off the trend, surprisingly showing lower value than for the Eu—Se bond. This is in accord with a perturbative estimate of the donor-acceptor stabilization energies in the B3LYP optimized complexes (Table S2), indicating lower $E^{(2)}$ values for the Eu—Te vs. Eu—Se interactions, which is not the case when the density functional with a higher exact-exchange admixture (e.g. B5050LYP) is used.

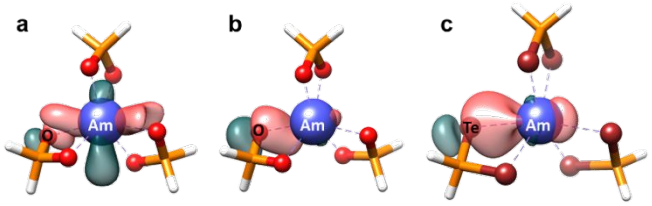

Figure 4: Formation of the dative Am—X (X = O, S, Se, Te) bond from natural hybrid orbitals in terms of a) overlapping O lone pair orbital of predominantly p character with the Am 6d hybridized orbital, which includes mixing of 7s and 5f character making it more directional toward the donor ligand; b) the final Am—O bonding NBO, which is mostly localized on O, indicating ionic character of the Am—ligand interactions. c) The coordinative σ Am—Te bonding NBO, which is increasingly polarized toward the Am ion, consistent with the increased basicity of the ligand. An isovalue of 0.05 e/A^3 was set for the NBOs rendering.

Summary and Conclusions

Efficient storage and processing of nuclear waste products requires the effective sequestration of trivalent lanthanides from actinides, despite the inherent difficulty in this separation due to similarities in ionic size. Following the promise of chalcogen-containing phosphinic acid ligands in performing this task, various theoretical methods were employed to replicate and elucidate high experimental separation factors from this class of compounds. However, previous studies enlisting several density functionals were at times at odds with one another and with empirical results. Thus, the body of literature on this topic abounds with competing interpretations of factors leading to effective Ln(III)/An(III) separation.

In an attempt to resolve these debates, we endeavored on a theoretical study of our own, of the efficacy of the model $H_2PX_2^-$ ligands, with X=O, S, Se, and Te, in the separation of the Am(III) ion from Eu(III). After first establishing an array of results from post-Hartree-Fock approaches as benchmarks, we set out to reveal which combination of density functional theory applications results in the best description of $Am(H_2PX_2)_3$ and $Eu(H_2PX_2)_3$ complexes, in terms of interatomic Am/Eu—X distances. Further, energies of reaction describing Am(III)/Eu(III) separation with these ligands were calculated in order to rank density functional theory approaches in their ability to predict relative selectivities.

With their prediction of greater Am—X than Eu—X interatomic distances for all X, density functionals with high exact-exchange admixtures successfully replicate MP2 benchmarks when used in conjunction with an f-in-valence description of metal ions. Moreover, this class of functionals results in the most consistent interatomic distance results for both Eu—X and Am—X complexes.

Functionals with large fractions of Hartree-Fock exchange also result in reaction energies most similar to those from benchmark CCSD(T) + δMP2 calculations. Not only do these functionals predict the same relative selectivity trends for ligands with respect to the choice of chalcogen in the ligand, but all reaction energies obtained from all these functionals when used in concert with a small-core approach, lie well within 1 kcal/mol of benchmarks.

Finally, we set to task elucidating electronic factors contributing to metal—ligand bonding in these complexes. A natural bond orbital analysis relates greater selectivity of Am(III) over Eu(III) in MP2 and B5050LYP calculations to a stronger change in forward dative sigma bonding in $Am(H_2PX_2)_3$ compared to $Eu(H_2PX_2)_3$ complexes in going from X = O to X= S, Se, and Te, as manifested in more strongly increased d-orbital (and to a lesser extent s-orbital) contributions to dative bonding by Am(III) over Eu(III) across the chalcogen series. Meanwhile, density functionals which perform poorly in terms of selectivity and complex structure tend to overfill valence f orbitals, more so in Eu(III) complexes than in Am(III) complexes.

We hope that our work in describing structural and bonding features of Ln— and An—soft-donor complexes resolves some of the discrepancies in theoretical descriptions pertaining to predicting Am/Ln selectivity. Further, in recommending a density functional with a high exact-exchange admixture in conjunction with an f-in-valence consideration of trivalent lanthanide and actinide ions, we anticipate the application of this type of approach towards accurate descriptions of complex structure and selectivity in future studies.

Author Contributions

Robert Chapleski: Investigation, Formal Analysis, Validation, Visualization, Writing – original draft. Alexander Ivanov: Investigation, Formal Analysis, Visualization, Writing – original draft. Kirk Peterson: Investigation, Formal Analysis, Methodology, Validation, Writing – original draft. Vyacheslav Bryantsev: Conceptualization, Funding Acquisition, Supervision, Project Administration, Resources, Writing – review & editing.

Conflicts of interest

There are no conflicts to declare.

Acknowledgements

This work was supported by the Nuclear Technology Research and Development Program, Office of Nuclear Energy, US Department of Energy. This research used resources of the National Energy Research Scientific Computing Center (NERSC) and the Computer and Data Environment for Science (CADES) at Oak Ridge National Laboratory, both of which are supported by the Office of Science, U.S. Department of Energy, under Contracts DEAC02-05CH11231 and DE-AC05-00OR22725, respectively. KAP was supported by the Heavy Element Chemistry Program, Office of Basic Energy Sciences, U.S. Department of Energy, Grant No. DE-SC0008501.

References

1. O. Ashraf and G. V. Tikhomirov, *Annals of Nuclear Energy*, 2020, **148**, 107751.
2. J. Chen, Y. Zhu and R. Jiao, *Separation Science and Technology*, 1996, **31**, 2723-2731.
3. Y. Zhu, J. Chen and R. Jiao, *Solvent Extraction and Ion Exchange*, 1996, **14**, 61-68.
4. G. Tian, Y. Zhu, J. Xu, T. Hu and Y. Xie, *Journal of Alloys and Compounds*, 2002, **334**, 86-91.
5. T. Guoxin, Z. Yongjun, X. Jingming, Z. Ping, H. Tiandou, X. Yaning and Z. Jing, *Inorganic Chemistry*, 2003, **42**, 735-741.
6. M. P. Jensen and A. H. Bond, *Journal of the American Chemical Society*, 2002, **124**, 9870-9877.
7. M. P. Jensen, A. H. Bond, P. G. Rickert and K. L. Nash, *Journal of Nuclear Science and Technology*, 2002, **39**, 255-258.
8. R. Shannon, *Acta Crystallographica Section A*, 1976, **32**, 751-767.
9. J. N. Cross, J. A. Macor, J. A. Bertke, M. G. Ferrier, G. S. Girolami, S. A. Kozimor, J. R. Maassen, B. L. Scott, D. K. Shuh, B. W. Stein and S. C. E. Stieber, *Angewandte Chemie International Edition*, 2016, **55**, 12755-12759.
10. A. J. Gaunt, S. D. Reilly, A. E. Enriquez, B. L. Scott, J. A. Ibers, P. Sekar, K. I. M. Ingram, N. Kaltsoyannis and M. P. Neu, *Inorganic Chemistry*, 2008, **47**, 29-41.
11. K. I. M. Ingram, M. J. Tassell, A. J. Gaunt and N. Kaltsoyannis, *Inorganic Chemistry*, 2008, **47**, 7824-7833.
12. K. I. M. Ingram, N. Kaltsoyannis, A. J. Gaunt and M. P. Neu, *Journal of Alloys and Compounds*, 2007, **444-445**, 369-375.
13. A. Bhattacharyya, T. K. Ghanty, P. K. Mohapatra and V. K. Manchanda, *Inorganic Chemistry*, 2011, **50**, 3913-3921.
14. M. Dolg, X. Cao and J. Ciupka, *Journal of Electron Spectroscopy and Related Phenomena*, 2014, **194**, 8-13.
15. X. Cao, D. Heidelberg, J. Ciupka and M. Dolg, *Inorganic Chemistry*, 2010, **49**, 10307-10315.
16. M. Dolg. *Journal of Chemical Theory and Computation,* 2011, **7**, 3131-3142.
17. A. Chandrasekar and T. K. Ghanty, *Inorganic Chemistry*, 2019, **58**, 3744-3753.
18. T. Sun, C. Xu, X. Xie, J. Chen and X. Liu, *ACS Omega*, 2018, **3**, 4070-4080.
19. X. Cao, J. Zhang, D. Weissmann, M. Dolg and X. Chen, *Physical Chemistry Chemical Physics*, 2015, **17**, 20605-20616.
20. M. Kaneko, S. Miyashita and S. Nakashima, *Inorganic Chemistry*, 2015, **54**, 7103-7109.
21. M. Kaneko, M. Watanabe, S. Miyashita and S. Nakashima, *Journal of Nuclear and Radiochemical Sciences*, 2017, **17**, 9-15.
22. M. Kaneko and M. Watanabe, *Journal of Radioanalytical and Nuclear Chemistry*, 2018, **316**, 1129-1137.
23. N. Pu, L. Xu, T. Sun, J. Chen and C. Xu, *Journal of Radioanalytical and Nuclear Chemistry*, 2019, **320**, 219-226.
24. Z. Wang, N. Pu, Y. Tian, C. Xu, F. Wang, Y. Liu, L. Zhang, J. Chen and S. Ding, *Inorganic Chemistry*, 2019, **58**, 5457-5467.
25. Y. Zhao and D. G. Truhlar, *Theoretical Chemistry Accounts*, 2008, **120**, 215-241.
26. N. P. Bessen, J. A. Jackson, M. P. Jensen and J. C. Shafer, *Coordination Chemistry Reviews*, 2020, **421**, 213446.
27. J. M. Keith and E. R. Batista, *Inorganic Chemistry*, 2012, **51**, 13-15.
28. B. Sadhu and M. Dolg, *Inorganic Chemistry*, 2019, **58**, 9738-9748.
29. S. R. Daly, J. M. Keith, E. R. Batista, K. S. Boland, D. L. Clark, S. A. Kozimor and R. L. Martin, *Journal of the American Chemical Society*, 2012, **134**, 14408-14422.
30. H.-J. Werner, P. J. Knowles, F. R. Manby, J. A. Black, K. Doll, A. Heßelmann, D. Kats, A. Köhn, T. Korona, D. A. Kreplin, Q. Ma, T. F. Miller, III, A. Mitrushchenkov, K. A. Peterson, I. Polyak, G. Rauhut and M. Sibaev, *The Journal of Chemical Physics*, 2020, **152**, 144107.
31. H.-J. Werner, *MOLPRO, version 2020.2, a package of ab initio programs, H.-J. Werner, P. J. Knowles, G. Knizia, F. R. Manby, M. Schütz, P. Celani, W. Györffy, D. Kats, T. Korona, R. Lindh, A. Mitrushenkov, G. Rauhut, K. R. Shamasundar, T. B. Adler, R. D. Amos, S. J. Bennie, A. Bernhardsson, A. Berning, D. L. Cooper, M. J. O. Deegan, A. J. Dobbyn, F. Eckert, E. Goll, C. Hampel, A. Hesselmann, G. Hetzer, T. Hrenar, G. Jansen, C. Köppl, S. J. R. Lee, Y. Liu, A. W. Lloyd, Q. Ma, R. A. Mata, A. J. May, S. J. McNicholas, W. Meyer, T. F. Miller III, M. E. Mura, A. Nicklass, D. P. O'Neill, P. Palmieri, D. Peng, T. Petrenko, K. Pflüger, R. Pitzer, M. Reiher, T. Shiozaki, H. Stoll, A. J. Stone, R. Tarroni, T. Thorsteinsson, M. Wang, and M. Welborn, see https://www.molpro.net.*
32. M. Douglas and N. M. Kroll, *Annals of Physics*, 1974, **82**, 89-155.
33. B. A. Hess, *Physical Review A*, 1986, **33**, 3742-3748.
34. M. Reiher and A. Wolf, *The Journal of Chemical Physics*, 2004, **121**, 10945-10956.
35. F. Neese, *WIREs Computational Molecular Science*, 2012, **2**, 73-78.
36. F. Neese, *WIREs Computational Molecular Science*, 2018, **8**, e1327.
37. F. Neese, F. Wennmohs, U. Becker and C. Riplinger, *The Journal of Chemical Physics*, 2020, **152**, 224108.
38. T. H. Dunning, Jr., *The Journal of Chemical Physics*, 1989, **90**, 1007-1023.
39. D. E. Woon and T. H. Dunning, Jr., *The Journal of Chemical Physics*, 1993, **98**, 1358-1371.

40. R. A. Kendall, T. H. Dunning, Jr. and R. J. Harrison, *The Journal of Chemical Physics*, 1992, **96**, 6796-6806.
41. K. A. Peterson, D. Figgen, E. Goll, H. Stoll and M. Dolg, *The Journal of Chemical Physics*, 2003, **119**, 11113-11123.
42. A. K. Wilson, D. E. Woon, K. A. Peterson and T. H. Dunning, Jr., *The Journal of Chemical Physics*, 1999, **110**, 7667-7676.
43. M. Dolg, H. Stoll and H. Preuss, *The Journal of Chemical Physics*, 1989, **90**, 1730-1734.
44. X. Cao and M. Dolg, *The Journal of Chemical Physics*, 2001, **115**, 7348-7355.
45. X. Cao and M. Dolg, *Journal of Molecular Structure: THEOCHEM*, 2002, **581**, 139-147.
46. W. Küchle, M. Dolg, H. Stoll and H. Preuss, *The Journal of Chemical Physics*, 1994, **100**, 7535-7542.
47. X. Cao, M. Dolg and H. Stoll, *The Journal of Chemical Physics*, 2003, **118**, 487-496.
48. X. Cao and M. Dolg, *Journal of Molecular Structure: THEOCHEM*, 2004, **673**, 203-209.
49. M. J. Frisch, G. W. Trucks, H. B. Schlegel, G. E. Scuseria, M. A. Robb, J. R. Cheeseman, G. Scalmani, V. Barone, G. A. Petersson, H. Nakatsuji, X. Li, M. Caricato, A. V. Marenich, J. Bloino, B. G. Janesko, R. Gomperts, B. Mennucci, H. P. Hratchian, J. V. Ortiz, A. F. Izmaylov, J. L. Sonnenberg, Williams, F. Ding, F. Lipparini, F. Egidi, J. Goings, B. Peng, A. Petrone, T. Henderson, D. Ranasinghe, V. G. Zakrzewski, J. Gao, N. Rega, G. Zheng, W. Liang, M. Hada, M. Ehara, K. Toyota, R. Fukuda, J. Hasegawa, M. Ishida, T. Nakajima, Y. Honda, O. Kitao, H. Nakai, T. Vreven, K. Throssell, J. A. Montgomery Jr., J. E. Peralta, F. Ogliaro, M. J. Bearpark, J. J. Heyd, E. N. Brothers, K. N. Kudin, V. N. Staroverov, T. A. Keith, R. Kobayashi, J. Normand, K. Raghavachari, A. P. Rendell, J. C. Burant, S. S. Iyengar, J. Tomasi, M. Cossi, J. M. Millam, M. Klene, C. Adamo, R. Cammi, J. W. Ochterski, R. L. Martin, K. Morokuma, O. Farkas, J. B. Foresman and D. J. Fox, *Journal*, 2016.
50. M. Dolg, H. Stoll, A. Savin and H. Preuss, *Theoretica chimica acta*, 1989, **75**, 173-194.
51. M. Dolg, H. Stoll and H. Preuss, *Theoretica chimica acta*, 1993, **85**, 441-450.
52. A. Moritz, X. Cao and M. Dolg, *Theoretical Chemistry Accounts*, 2007, **117**, 473-481.
53. F. Weigend, M. Häser, H. Patzelt and R. Ahlrichs, *Chemical Physics Letters*, 1998, **294**, 143-152.
54. F. Weigend and M. Häser, *Theoretical Chemistry Accounts*, 1997, **97**, 331-340.
55. M. Feyereisen, G. Fitzgerald and A. Komornicki, *Chemical Physics Letters*, 1993, **208**, 359-363.
56. D. E. Bernholdt and R. J. Harrison, *Chemical Physics Letters*, 1996, **250**, 477-484.
57. F. Neese, F. Wennmohs, A. Hansen and U. Becker, *Chemical Physics*, 2009, **356**, 98-109.
58. F. Weigend, A. Köhn and C. Hättig, *The Journal of Chemical Physics*, 2002, **116**, 3175-3183.
59. C. Hättig, G. Schmitz and J. Koßmann, *Physical Chemistry Chemical Physics*, 2012, **14**, 6549-6555.
60. F. Weigend, *Journal of Computational Chemistry*, 2008, **29**, 167-175.
61. G. L. Stoychev, A. A. Auer and F. Neese, *Journal of Chemical Theory and Computation*, 2017, **13**, 554-562.
62. Q. Lu and K. A. Peterson, *The Journal of Chemical Physics*, 2016, **145**, 054111.
63. R. Feng and K. A. Peterson, *The Journal of Chemical Physics*, 2017, **147**, 084108.
64. W. A. de Jong, R. J. Harrison and D. A. Dixon, *The Journal of Chemical Physics*, 2001, **114**, 48-53.
65. T. H. Dunning, Jr., K. A. Peterson and A. K. Wilson, *The Journal of Chemical Physics*, 2001, **114**, 9244-9253.
66. J. P. Perdew, K. Burke and M. Ernzerhof, *Physical Review Letters*, 1996, **77**, 3865-3868.
67. S. Lehtola, C. Steigemann, M. J. T. Oliveira and M. A. L. Marques, *SoftwareX*, 2018, **7**, 1-5.
68. J.-D. Chai and M. Head-Gordon, *The Journal of Chemical Physics*, 2008, **128**, 084106.
69. S. Grimme, *Journal of Computational Chemistry*, 2006, **27**, 1787-1799.
70. Y. Shao, M. Head-Gordon and A. I. Krylov, *The Journal of Chemical Physics*, 2003, **118**, 4807-4818.
71. Y. A. Bernard, Y. Shao and A. I. Krylov, *The Journal of Chemical Physics*, 2012, **136**, 204103.
72. D. A. Pantazis and F. Neese, *Journal of Chemical Theory and Computation*, 2009, **5**, 2229-2238.
73. D. A. Pantazis and F. Neese, *Journal of Chemical Theory and Computation*, 2011, **7**, 677-684.
74. D. H. Bross and K. A. Peterson, *Theoretical Chemistry Accounts*, 2013, **133**, 1434.
75. E. D. Glendening, J. K. Badenhoop, A. E. Reed, J. E. Carpenter, J. A. Bohmann, C. M. Morales, P. Karafiloglou, C. R. Landis and F. Weinhold, *Journal*, 2018.
76. J. P. Foster and F. Weinhold, *Journal of the American Chemical Society*, 1980, **102**, 7211-7218.
77. K. B. Wiberg, *Tetrahedron*, 1968, **24**, 1083-1096.
78. A. E. Reed, L. A. Curtiss and F. Weinhold, *Chemical Reviews*, 1988, **88**, 899-926.
79. M. P. Jensen and A. H. Bond, *Radiochimica Acta*, 2002, **90**, 205-209.
80. D. Manna and T. K. Ghanty, *Physical Chemistry Chemical Physics*, 2012, **14**, 11060-11069.
81. A. Karton and J. M. L. Martin, *Theoretical Chemistry Accounts*, 2006, **115**, 330-333.
82. J. M. L. Martin, *Chemical Physics Letters*, 1996, **259**, 669-678.
83. Y. Zhu, J. Chen and G. R. Choppin, *Solvent Extraction and Ion Exchange*, 1996, **14**, 543-553.
84. J. G. Hill and K. A. Peterson, *The Journal of Chemical Physics*, 2017, **147**, 244106.